Stacking-driven gap formation in layered 1*T*-TaS_2

T. Ritschel*
Quantum Matter Institute, The University of British Columbia, 2355 East Mall, Vancouver B.C., V6T 1Z4, Canada

H. Berger
Ecole polytechnique Federale de Lausanne, Switzerland

J. Geck
Institute of Solid State and Materials Physics, TU-Dresden, 01062 Dresden, Germany

(Received 5 June 2018; published 26 November 2018)

The layered transition metal dichalcogenides which show an inherent tendency towards charge density wave order are traditionally considered to realize rather two-dimensional electronic systems. However, recent theoretical and experimental results suggest that the stacking of the charge density wave and related orbital order in the direction perpendicular to the layers plays a key role for the in-plane electronic structure. Here we present a state-of-the-art density functional theory (DFT) study which models crucial features of the partially disordered orbital order stacking in the prototypical layered transition metal dichalcogenide 1*T*-TaS_2. We show that a DFT model with realistic assumptions about the orbital order perpendicular to the layers yields band structures which agree remarkably well with experiments and also correctly predicts the formation of an excitation gap at the Fermi energy. Our results not only imply that the widely accepted paradigm of local Mott physics as the driving mechanism behind the gap formation in 1*T*-TaS_2 needs to be reconsidered but they also highlight the crucial role of interlayer interactions in layered transition metal dichalcogenides in general.

DOI: 10.1103/PhysRevB.98.195134

I. INTRODUCTION

The spontaneous formation of so-called electronic crystals, i.e., spatial superlattices formed collectively by the valence electrons of a solid is among the most striking topics in current condensed matter research [1,2]. Charge density wave (CDW) order is a manifestation of such macroscopic collective quantum states which occurs in a wide range of materials, including doped copper oxide systems [3,4], heavy fermion systems [5], or layered transition metal dichalcogenides (TMDs) [6]. In particular the latter class of materials currently regains enormous attention as "post-graphene" quasi-two-dimensional materials. Their unusual electronic properties propel innovative concepts for applications ranging from miniaturized electronic devices to quantum computing [7–11].

Owing to the weak bonding between the layers, the TMDs are traditionally considered to realize rather two-dimensional electronic systems. However, recent theoretical and experimental work suggests that, due to orbital order which is intertwined with the CDW, the electronic structure markedly depends on the stacking arrangement of this combined order in the direction perpendicular to the layers [12–19]. Accordingly, density functional theory (DFT) based on oversimplified assumptions about the CDW stacking will yield electronic structures that do not agree with experiment [15]. In this paper we present a DFT model that realistically approximates the experimentally found partially disordered CDW stacking for the prototypical material 1*T*-TaS_2 and compare these calculations to detailed angle resolved photoemission spectroscopy data. 1*T*-TaS_2 serves here as a prime example to study the effect of interlayer correlations in the quasi-2D TMDs.

Among the TMDs 1*T*-TaS_2 is well known for its particularly rich electronic phase diagram as a function of temperature and pressure [20]. Starting at ambient pressure and low temperatures the in-plane (IP) CDW order is commensurate (C) with the underlying crystal lattice. It is characterized by star-of-david shaped clusters comprising 13 Tantalum sites arranged in a $\sqrt{13} \times \sqrt{13}$ IP superstructure as illustrated in Fig. 1(a). Increasing the temperature or rising the external pressure yields a so-called nearly commensurate (NC)-CDW which is associated with the creation of defects within the C-CDW which, by themselves, order on a yet larger length scale [21]. At higher temperatures or pressures the NC-CDW transforms into incommensurate (IC)-CDWs. In addition to this variety of CDWs, 1*T*-TaS_2 also features pressure induced superconductivity above $\approx$3 GPa and below 5 K [20].

A remarkable feature of 1*T*-TaS_2, which has sparked immense research efforts over the past 40 years, lies in the semiconducting transport properties of its C-CDW phase. A semiconducting CDW phase is very uncommon among the class of TMDs. All other CDW phases are metallic or even superconducting at low temperatures [6,22]. Commonly, the semiconducting C-CDW is attributed to Mott-Hubbard type electron-electron correlations. According to this scenario every star-of-David cluster contributes a single 5*d* electron

*tobias.ritschel@posteo.org

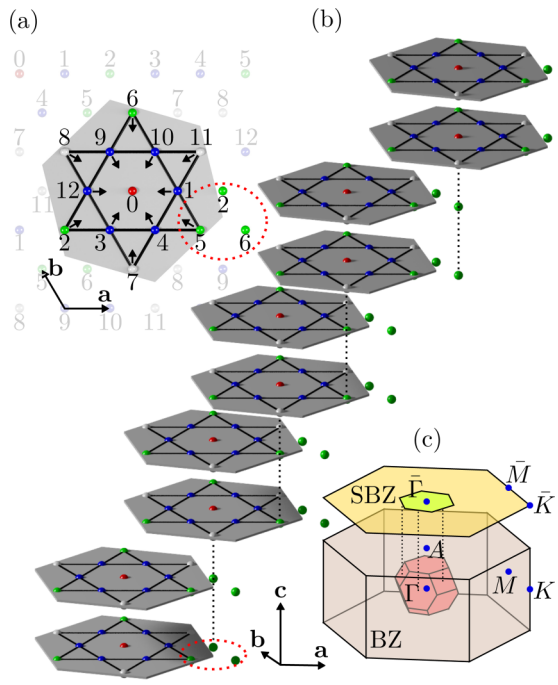

FIG. 1. CDW layer stacking of the C-CDW in 1*T*-TaS_2. (a) The star-of-david shaped in-plane $\sqrt{13} \times \sqrt{13}$ supercell comprises clusters of 13 Ta sites (gray hexagon). (b) The $\mathbf{t}_{0(2,5,6)}$ stacking of these clusters in the out-of-plane direction is given by on-top stacked bilayers which by themselves are stacked by a vector randomly chosen from three symmetry equivalent vectors corresponding to the green sites in (a). The normal cell lattice vectors are indicated (**a**, **b**, **c**). (c) The bulk Brillouin zone (BZ) and surface Brillouin zone (SBZ) corresponding to the normal cell and the supercell of the approximated periodic stacking $\mathbf{t}_{02}$.

to a half filled narrow conduction band. A sufficiently large Coulomb repulsion U acting on these clusters is believed to drive a cluster Mott-Hubbard transition with overlapping Hubbard subbands [23,24]. It has been proposed that Anderson localization finally drives a metal-to-insulator transition at low temperatures yielding the observed semiconducting transport properties [25,26]. Recently, time- and angle-resolved photoemission spectroscopy (trARPES) was employed to observe the ultrafast collapse of an excitation gap at the Brillouin zone center [Γ point, cf. Fig. 1(c)]—the so-called Mott gap—which was interpreted as a clear signature that electronic degrees of freedom are involved in the formation of this gap [27–29].

Based on this widely accepted cluster Mott-physics scenario Law and Lee [30] lately suggested that 1*T*-TaS_2 should be considered as a candidate for the realization of a quantum spin liquid (QSL)—an exotic state of matter in which the quantum spins refrain to order even at $T = 0$ K [31]. This exciting proposal initiated considerable interest in searching for signatures of the QSL state [32–35]. However, compelling evidence for the existence of the QSL state has so far eluded experimental confirmation. In addition, interlayer coupling, which we will show to be significant in this material, complicate the QSL interpretation of the C-CDW phase in 1*T*-TaS_2 [30,35].

An important fact that is often overlooked is that not only the IP structure is affected by the transitions between the different CDWs but also the stacking arrangement in the out-of-plane (OP) direction. The IC-CDW and the NC-CDW possess a well-ordered stacking along the OP direction with a periodicity corresponding to three times the layer-to-layer distance $c_0 \approx 5.9$ Å [21]. In contrast, the C-CDW is governed by a complex alternating and partially disordered stacking along the OP direction: According to the 13 Tantalum sites forming one star-of-david cluster [labels 0 . . . 12 in Fig. 1(a)], there are 13 possibilities of how two adjacent layers are aligned with respect to each other. We introduce the following notation: An arrangement where the central site, i.e., site 0, within a star-of-David cluster is centered above site $i \in (0 \ldots 12)$ in the layer below is referred to as $\mathbf{t}_i$. Taking the threefold IP symmetry of the C-CDW into account the 13 distinct stacking types form five symmetry equivalent groups, namely $\mathbf{t}_{(2,5,6)}$, $\mathbf{t}_{(7,8,11)}$, $\mathbf{t}_{(1,3,9)}$, $\mathbf{t}_{(4,10,12)}$, and $\mathbf{t}_0$. Although the stacking of the C-CDW in 1*T*-TaS_2 is still debated, there is firm theoretical [36,37] and experimental [15,38–41] evidence that it can be viewed as bilayers which are stacked on top, i.e., stacking $\mathbf{t}_0$. These bilayers, for their part, are stacked by a random choice out of the three symmetry equivalent possibilities corresponding to the group $\mathbf{t}_{(2,5,6)}$. The resulting alternating partially disordered stacking, which we will denote by $\mathbf{t}_{0(2,5,6)}$, is illustrated in Fig. 1(b). Embedded in this strictly alternating stacking are defects which may result in single (unpaired) layers [15,41]. To the best of our knowledge, the peculiar disordered C-CDW stacking is only found in 1*T*-TaS_2. The closely related material 1*T*-$TaSe_2$ develops the same $\sqrt{13} \times \sqrt{13}$ IP C-CDW structure. However, in this material the stacking is governed by the formation of macroscopic domains with a long-range ordered stacking corresponding to one stacking out of the group $\mathbf{t}_{(2,5,6)}$ [42]. Interestingly, it has been shown that this long-range OP stacking order can be transformed into a disordered stacking among the group $\mathbf{t}_{(2,5,6)}$ by subtle doping of Zr impurities on the Ta site [43]. However, as opposed to 1*T*-TaS_2 there is no alternation between different stacking groups.

II. RESULTS

1. DFT band structure calculations

Previous theoretical studies of the electronic structure of the C-CDW in 1*T*-TaS_2 have, apart from a few exceptions (Refs. [12,44]), widely ignored the CDW stacking in the OP direction. In what follows we will use an extension of our previous DFT approach (Ref. [15]) to show that the transport properties and in particular the gap at Γ of the C-CDW phase can indeed be explained by correctly modeling the actual CDW stacking.

All first-principle calculations have been done using the FPLO package (versions 14 and 18) [45]. Following our previous approach the IP supercell structure was derived from Refs. [21,46]. In order to incorporate the different stacking types we constructed triclinic supercells without changing the atomic displacements and using the experimental interlayer distance $c_0 = 5.91$ Å [46]. We used the generalized gradient approximation (GGA) and the local density approximation

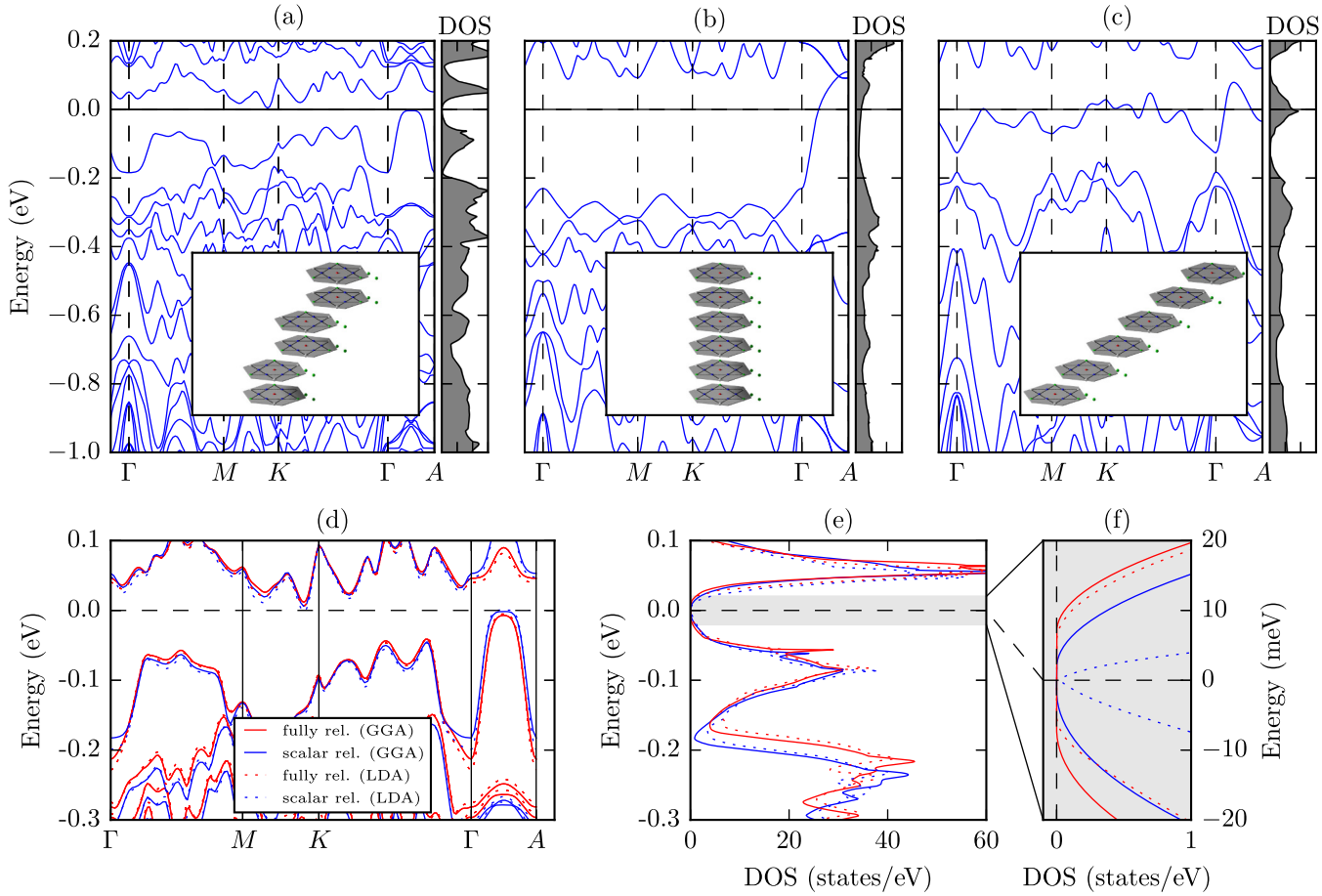

FIG. 2. (a)–(c) DFT band structure and density of states for the same in-plane supercell but different stacking types (GGA and scalar relativistic). (a) The alternating stacking $\mathbf{t}_{02}$. (b) The on-top stacking $\mathbf{t}_0$. (c) The nonalternating stacking $\mathbf{t}_2$. Illustrations of the different stacking types are given in the insets, respectively. (d)–(f) DFT band structure (d) and density of states [(e) and (f)] of the $\mathbf{t}_{02}$ stacking for GGA (solid lines) and LDA (dotted lines) in scalar relativistic (blue) and fully relativistic (red) treatment of the Kohn-Sham problem. A magnification of the highlighted energy range around the Fermi level in (e) is shown in (f). The high-symmetry points in all band structure plots correspond to the normal cell Brillouin zone [cf. Fig. 1(c)].

(LDA) of the exchange-correlation potential as parametrized by Perdew, Burke, and Ernzerhof (Ref. [47]) and Perdew and Wang (Ref. [48]), respectively. For the fully relativistic calculations the full four-component Dirac-Kohn-Sham theory as implemented in FPLO was employed [49]. The total density was converged on a grid of $4 \times 4 \times 4$ irreducible k points. For the density of states calculation we used a denser grid of $12 \times 12 \times 12$ k points. Brillouin zone integration was done using the tetrahedron method.

The disordered alternating stacking of the C-CDW as illustrated in Fig. 1(b) does not obey translational symmetry in the OP direction and, hence, it cannot be treated in a conventional DFT band structure scheme. In order to circumvent this difficulty we approximate the disordered stacking by a periodic alternation of the stacking $\mathbf{t}_0$ and $\mathbf{t}_2$. In other words, the partial disorder among the group of symmetry equivalent stacking types $\mathbf{t}_{(2,5,6)}$ is neglected and a single fixed stacking $\mathbf{t}_2$ is chosen. We denote this stacking, which is visualized in the inset of Fig. 2(a), by $\mathbf{t}_{02}$. In Fig. 2(a) we show the result of a scalar relativistic DFT band structure calculation within the generalized gradient approximation (GGA) for this periodically alternating stacking. For comparison we also reproduce the band structure calculations from Ref. [15] for the nonalternating stacking types $\mathbf{t}_0$ and $\mathbf{t}_2$ in Figs. 2(b) and 2(c), respectively.

The first and most important observation is that the DFT calculation which takes the alternating stacking into account indeed yields a gaplike feature at the Fermi energy. This can be most clearly seen from the density of states (DOS) shown in the right panel of Fig. 2(a). Thus, the key result of these calculations is that DFT predicts an insulating or semiconducting ground state for the alternating stacking $\mathbf{t}_{02}$. In contrast, the nonalternating stacking types $\mathbf{t}_0$ and $\mathbf{t}_2$ possess a Fermi surface and, hence, our DFT calculations predict metallic ground states [cf. Figs. 2(b) and 2(c)] in accordance with previous calculations [12,14,15,44,50].

2. Stacking-induced small-gap semiconductor

Although the formation of this gap is surprising at first glance it can be understood in terms of elementary band theory arguments: The supercell corresponding to stacking $\mathbf{t}_0$ or $\mathbf{t}_2$ contains an odd number of electrons (13 Tantalum sites each contributing one $5d$ electron). DFT calculations for these

stacking types result in metallic ground states as the valence band is partially filled. In order to model the alternating stacking it is necessary to include two star-of-David clusters in the supercell. Accordingly, the resulting even number of electrons in this supercell can yield a completely filled valence band and thus an insulating or semiconducting ground state as already pointed out more than 30 years ago by Naito *et al.* [40]. However, this line of arguments does certainly not allow us to deduce the size of the gap. Depending on subtle details of the hopping integrals between wave functions in adjacent layers the gap size could indeed be very small, zero or there could even be a small overlap of valance and conduction band resulting in a semimetal with conducting behavior at finite temperatures. The band structure and DOS shown in Fig. 2(a) indicate a small-gap semiconductor with a gap size of about 3 meV for the case of the $\mathbf{t}_{02}$ stacking. Noteworthy, bulk crystals of the closely related material 1*T*-$TaSe_2$ which possesses the same IP C-CDW structure as 1*T*-TaS_2 but assumes the $\mathbf{t}_2$ (and symmetry equivalent) stacking, remain metallic at low temperatures [51,52]. This experimental fact further corroborates our findings that the CDW stacking is key for the electronic gap structure in these materials. In the following section we will discuss the robustness of the gap induced by the $\mathbf{t}_{02}$ stacking with respect to the level of approximation used in the calculations.

3. *Effect of spin-orbit coupling*

The calculations shown in Fig. 2(a)–2(c) are carried out in a scalar relativistic approximation, hence they are neglecting the spin-orbit interaction which might be significant as Tantalum is a rather heavy element. In Figs. 2(d)–2(f) we show the band structure and the DOS close to the Fermi energy for a fully relativistic calculation including spin-orbit coupling in comparison to the scalar relativistic result. The band structures shown in Fig. 2(d) reveal that the effect introduced by spin-orbit coupling is limited to rather small band shifts and splittings in the range of a few meV. Yet these subtle modifications indeed further open the (indirect) band gap at the Fermi energy to about 14 meV as can be clearly observed in the magnified DOS shown in Fig. 2(f). Interestingly, recent transport measurements indicate that the temperature dependence of the electrical resistivity between 140 K and 40 K in the C-CDW phase of 1*T*-TaS_2 is well described by an excitation energy of about 112 K $\approx$ 10 meV which is of the same order as the gap size we find in our calculations [53].

It has been argued previously that spin-orbit coupling might be the key ingredient for the formation of a narrow band at the Fermi level which serves as a starting point for the proposed Mott-Hubbard-type metal-to-insulator transition [54]. The current calculations instead suggest that the particular CDW-layer stacking in combination with spin-orbit coupling is sufficient to open a gap at the Fermi level.

It should be noted that the actual size of the gap also depends on the approximation of the exchange-correlation potential. For instance a calculation within the local density approximation (LDA) merely results in a reduction of the DOS to zero in a single point at the Fermi energy compatible with a zero-gap semiconductor [see blue dotted line in Fig. 2(f)]. Similar to the calculations within the GGA the inclusion of spin-orbit coupling opens a gap of about 10 meV also for the LDA [red dotted line in Fig. 2(f)]. Likewise the interlayer distance has an influence of the gap size. However, the main result, that the $\mathbf{t}_{02}$ stacking gives rise to a gap at the Fermi energy, remains untouched by these technical details.

4. *In-depth comparison to angle-resolved photoemission spectroscopy*

We will now assess the validity of our DFT model of the C-CDW phase by a detailed comparison of the calculated electronic band structure to angle-resolved photoemission spectroscopy (ARPES) measurements. To this end we have measured the valance electronic structure of a high quality single crystal of 1*T*-TaS_2 as a function of k_x and k_y which, together with the energy axis, yields a 3D data set.

For this 3D data set we used *p*-polarized light of 96 eV photon energy, so that the final state crystal momentum at normal emission corresponds to the Γ point [55,56]. In order to gain insights about the k_z dependence of the electronic structure we also measured the ARPES signal along selected high-symmetry directions of the BZ with light of 84 eV photon energy. For this photon energy the initial state crystal momentum at normal emission corresponds approximately to the point halfway between Γ and A $(0,0,\pi/2c_0)$ of the normal cell bulk BZ [see Fig. 1(c)] [56]. For all measurements the sample temperature was kept at 1 K.

In Figs. 3(f)–3(k) we present various constant energy cuts through the 3D data set while Figs. 3(k)–3(n) show cuts along high symmetry directions of the BZ. Figures 3(m) and 3(n) show the spectral feature around the Fermi energy and close to normal emission for the two different photon energies. Overall, our experimental data agree well with previously reported ARPES studies of the C-CDW in 1*T*-TaS_2 [22,29,50,56,57].

In order to enable a comparison of the theoretical band structures to the experimentally accessible spectral function $\mathcal{A}(k,\omega)$ [58] we use the unfolding scheme as described in Ref. [59] for our fully relativistic DFT model. The unfolded band structures corresponding to $k_z = 0$ and $k_z = \pi/2c_0$ are shown as magenta and blue overlays in Figs. 3(f)–3(n), respectively.

In Figs. 3(a)–3(e) we use these unfolded band structures to simulate a spectral function based on a heuristic approximation in order to mimic the effect of the partial disorder which is a marked characteristic of the CDW stacking in 1*T*-TaS_2: Since the three vectors $\mathbf{t}_2$, $\mathbf{t}_5$, and $\mathbf{t}_6$ occur randomly in the partially disordered stacking, the whole structure obeys, on average, threefold rotational symmetry. As can be clearly seen from the band weights shown in Figs. 3(f)–3(k) this threefold symmetry is broken by the approximation $\mathbf{t}_{02}$, which has only inversion symmetry. We have therefore symmetrized the calculated unfolded band structure for $\mathbf{t}_{02}$ in order to restore the threefold symmetry. This symmetrization bears on the assumption that, on average, the effect of the disorder on the electronic structure can be approximated with a linear incoherent superposition of $\mathbf{t}_{02}$, $\mathbf{t}_{05}$, and $\mathbf{t}_{06}$. In addition, it is known that ARPES spectra often represent an inherent k_z integration of the electronic structure [60]. In other words, the k_z momentum of the electrons which are probed by an ARPES

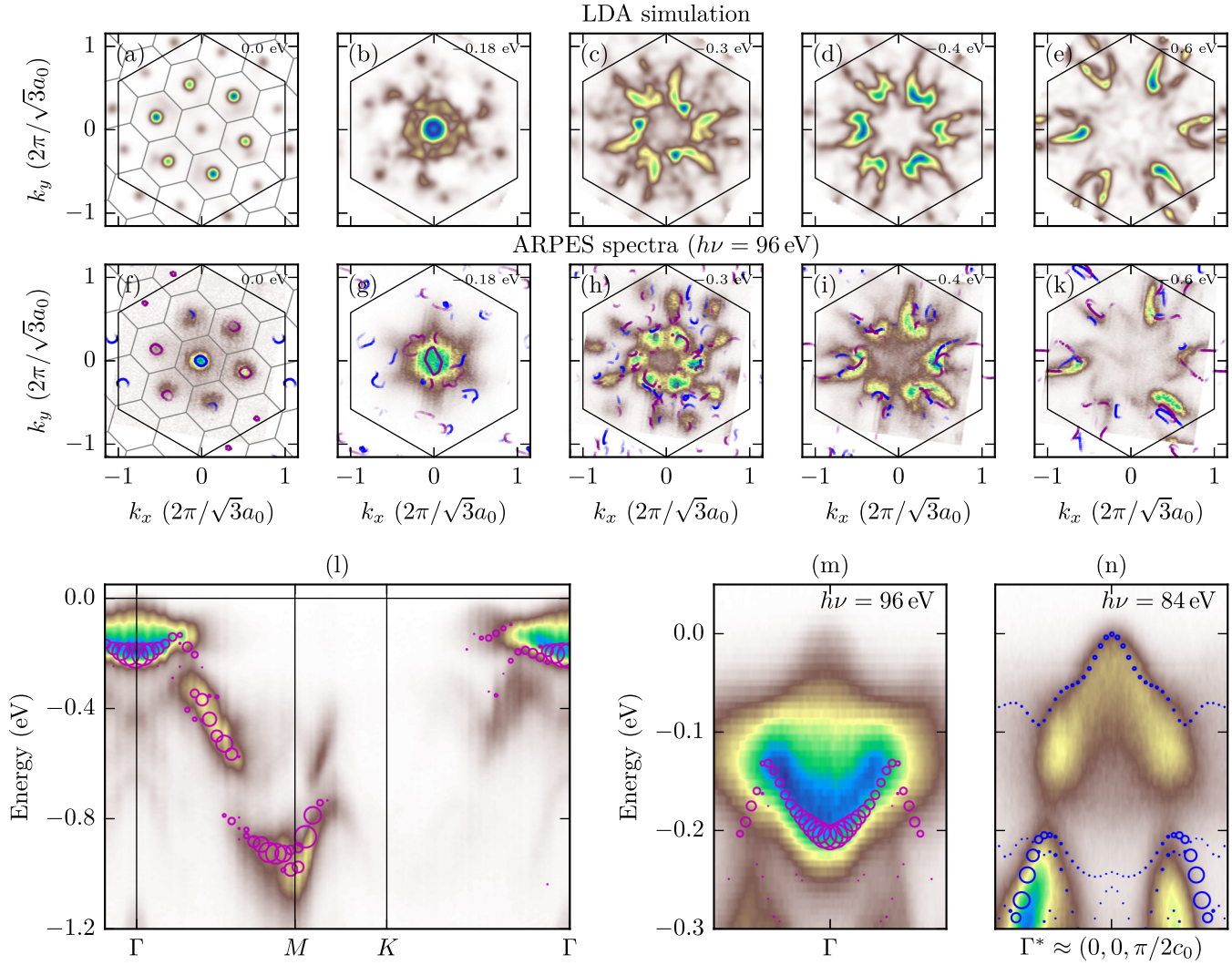

FIG. 3. Comparison of the theoretical electronic band structure corresponding to the $\mathbf{t}_{02}$ stacking with ARPES data. (a)–(k) Constant energy cuts (energy is indicated in the top right corner of the graphs) through the simulated spectral function [(a)–(e)] in comparison to the ARPES data [(f)–(k)]. Thick and thin solid black lines in (a) and (f) indicate the surface Brillouin zone boundaries corresponding to the normal cell and supercell, respectively. $a_0 = 3.36$ Å and $c_0 = 5.91$ Å are the lattice parameter of the undistorted crystal structure. (l) ARPES data ($h\nu = 96$ eV) along high symmetry directions of the normal cell surface Brillouin zone [cf. Fig. 1(c)]. (m) Magnification of the region around the Fermi energy and close to the Γ point in (l). (n) Same as (m) but for photon energy $h\nu = 84$ eV. Blue and magenta symbols in (f)–(n) indicate the unfolded band structure for $k_z = 0$ and $k_z = \pi/2c_0$, respectively. The contour lines in (f) correspond to an energy of 20 meV below the Fermi level.

experiment is not sharply defined. Thus electrons with different k_z momenta additionally contribute to the photocurrent. This effect can be clearly observed for instance in Fig. 3(f) where the spectral feature in the center of the BZ is likely to originate from a band corresponding to $k_z = \pi/2c_0$ (blue lines) while the six surrounding spots coincide with bands corresponding to $k_z = 0$ (magenta lines). For the simulated spectral function shown in Figs. 3(a)–3(e) we thus consider a weighted linear combination of unfolded IP band structures corresponding to six equidistant k_z values between $k_z = 0$ and $k_z = \pi/2c_0$. The weighting factors follow a Gaussian distribution centered at Γ. Finally, the unfolded band structure is convoluted with a resolution function in order to obtain the simulated spectral function shown in Figs. 3(a)–3(e). Note that the present DFT simulation does not account for more elaborate matrix element effects [61] of the photoemission process, causing deviations between DFT simulation and experiment. However, these deviations play no role for the following discussion.

III. DISCUSSION

In fact, apart from details in the intensity distribution and minor renormalizations of the binding energies, the overall agreement between measurement and calculation in Fig. 3 is remarkable. For instance, not only the energy of the electron pocket feature at the Γ point is rather well reproduced by our calculations [Figs. 3(l) and 3(m)]. Also the shape of that feature is nicely described by the DFT model. This is remarkable as these bands are rendered holelike for the nonalternating

stacking types [Figs. 2(b) and 2(c)]. It should be emphasized that the gap between the center of this feature at the Γ point and the Fermi level is commonly explained in terms of electron-electron correlations and is therefore often referred to as the "Mott gap." This interpretation is indeed corroborated by the ultrafast response of this gap to photoexcitation, which appears inconsistent with a gap caused by electron-phonon interactions [27–29,62].

Notwithstanding, the quantitatively correct prediction of this feature by pure DFT, i.e., not DFT+U, strongly argues against local Mott physics as the origin of the gap at the Γ point. Although the theoretical binding energy of the electron pocked is about 5 meV too large compared to the ARPES data it is more likely that the intrinsic disorder in this material is responsible for the renormalization rather than electron-electron correlations which usually tend to increase excitation gaps. Thus, our results give robust evidence that this gap at the Γ point is indeed primarily governed by interlayer hybridization and that electron-electron correlations solely play a secondary role. The marked sensitivity of the low-energy electronic structure with respect to the OP order found here is indeed rooted in orbital textures, which are interwoven with the CDW [12,15]. Different stacking arrangements alter the hopping integrals between the orbitally ordered layers in a nontrivial manner yielding pronounced changes in the electronic structure. It is important to point out that the electronic orbitals can respond to external perturbations on electronic time scales, i.e., our result is in keeping with the observed ultrafast response of the gap at Γ.

The energy cuts at the Fermi level (Fermi surface) shown in Figs. 3(a) and 3(f) imply another interesting result: The weak signal observed in ARPES was previously referred to as a remnant or pseudogapped Fermi surface [25,63–65]. Surprisingly, similar features occur in our DFT calculations [cf. Fig. 3(a)]. The finite intensity at the Γ point in the simulation shown in Fig. 3(a) is a result of the k_z integration (in combination with the finite energy broadening): The electron pocket at the Γ point transforms into a holelike band as k_z increases towards the A point. This trend is not only predicted by our calculations but also clearly observed experimentally as demonstrated in Figs. 3(m) and 3(n) which shows the unfolded band structures for $k_z = 0$ and $k_z = \pi/2c_0$ along with ARPES measurements at photon energies nominally corresponding to these k_z values. It is interesting to note that the k_z dispersion is overestimated by the present calculation. This deviation is again likely to stem from the disorder found in the real material which should reduce the bandwidth. Strictly speaking, k_z is not a good quantum number in this system anymore, although photon energy dependent ARPES reveals clear k_z dispersion [56] [see also Figs. 3(m) and 3(n)]. Accordingly, the pseudogap feature, which is observed in ARPES at photon energies nominally corresponding to the Γ point, might be directly related to the partial disorder of the CDW stacking in 1T-TaS_2, as this breaks the translational symmetry in the OP direction, causing a pronounced broadening in the k_z direction and yielding similar effects as the k_z integration performed here.

In view of the recent discussion about 1T-TaS_2 being a QSL candidate our results seem to question the very foundation of this proposal at least for the bulk material. Law and Lee (Ref. [30]) argued that even for nonvanishing interlayer coupling the QSL ground state could survive if it is fully gapped on each layer and if the interlayer hopping is sufficiently small. However, in our calculations the interlayer hopping is of the order of ≈200 meV [cf. Fig. 2(d)] which is in line with our ARPES measurements shown in Figs. 3(m) and 3(n) and previous energy dependent ARPES studies [56]. Thus we believe that purely 2D models are certainly not sufficient to capture the physics of the C-CDW in 1T-TaS_2. On the other hand, in the monolayer limit, when interlayer couplings, of course, vanish, the proposed Mott physics could become dominating again as DFT predicts a very narrow well-isolated and half-filled band at the Fermi energy which is prone to Mott localization [14]. Based on this notion one might speculate that stacking faults which interrupt the random stacking of $\mathbf{t}_0$ bilayers could leave behind well-separated unpaired layers effectively acting as embedded monolayers. Experiments indicate that such defects indeed exist [15,41,66,67]. These embedded monolayers could then in principle support Mott physics and QSL physics and could give, hence, rise to the observed anomalies in recent nuclear magnetic resonance, specific heat, and thermal conductivity measurements which were interpreted as signatures of the QSL state [32–34].

In conclusion, we presented DFT calculations for the C-CDW phase of 1T-TaS_2, which reproduce all the main features of the experimentally observed electronic structure on a quantitative level. The key ingredient for the presented supercell calculations is a realistic description of the OP stacking. Strong local electron-electron correlations are therefore not necessary to understand the general features of the electronic structure of 1T-TaS_2 in the C-CDW phase. In particular the so-called Mott gap can be explained *quantitatively* by the hybridization of orbitally ordered *ab* planes stacked along the *c* direction instead of local electron-electron interactions which indeed challenges the long-standing paradigm of Mott physics as the key mechanism for the formation of this gap at Γ. As a result, despite the layered structure of the TMDs, the OP stacking plays a dominant role for the IP electronic (gap) structure and, hence, the transport properties. Finally we showed that the strong interlayer couplings predicted by our calculations are generally in contradiction with the recently proposed QSL ground state which might characterize the C-CDW of 1T-TaS_2. However, in the limit of monolayers, which effectively could also exist in the bulk material due to CDW stacking faults, Mott physics, and QSL physics might still play an important role. Recent advances in the preparation of ultrathin samples for instance by mechanical exfoliation or by controlled growth using molecular beam epitaxy pave the way to scrutinize this intriguing possibility.

ACKNOWLEDGMENTS

This work was financially supported by the Deutsche Forschungsgemeinschaft under Grants No. RI 2908/1-1, No. DFG-GRK1621, and No. GE 1647/2-1. We acknowledge fruitful discussion with K. Rossnagel, G. Sawatzky, and K. Koepernik. For support during the synchrotron experiments we would like to thank J. Trinckauf.

[1] P. Monceau, Adv. Phys. **61**, 325 (2012).
[2] G. Grüner, *Density Waves in Solids* (Addison-Wesley, Reading, MA, 1994), Vol. 89.
[3] L. Chaix, G. Ghiringhelli, Y. Y. Peng, M. Hashimoto, B. Moritz, K. Kummer, N. B. Brookes, Y. He, S. Chen, S. Ishida, Y. Yoshida, H. Eisaki, M. Salluzzo, L. Braicovich, Z.-X. Shen, T. P. Devereaux, and W.-S. Lee, Nat. Phys. **13**, 952 (2017).
[4] J. Chang, E. Blackburn, A. T. Holmes, N. B. Christensen, J. Larsen, J. Mesot, R. Liang, D. A. Bonn, W. N. Hardy, A. Watenphul, M. v. Zimmermann, E. M. Forgan, and S. M. Hayden, Nat. Phys. **8**, 871 (2012).
[5] T. Gruner, D. Jang, Z. Huesges, R. Cardoso-Gil, G. H. Fecher, M. M. Koza, O. Stockert, A. P. Mackenzie, M. Brando, and C. Geibel, Nat. Phys. **13**, 967 (2017).
[6] J. Wilson, F. Di Salvo, and S. Mahajan, Adv. Phys. **24**, 117 (1975).
[7] L. Stojchevska, I. Vaskivskyi, T. Mertelj, P. Kusar, D. Svetin, S. Brazovskii, and D. Mihailovic, Science **344**, 177 (2014).
[8] M. Yoshida, R. Suzuki, Y. Zhang, M. Nakano, and Y. Iwasa, Sci. Adv. **1**, e1500606 (2015).
[9] I. Vaskivskyi, I. A. Mihailovic, S. Brazovskii, J. Gospodaric, T. Mertelj, D. Svetin, P. Sutar, and D. Mihailovic, Nat. Commun. **7**, 11442 (2016).
[10] L. Ma, C. Ye, Y. Yu, X. F. Lu, X. Niu, S. Kim, D. Feng, D. Tománek, Y.-W. Son, X. H. Chen, and Y. Zhang, Nat. Commun. **7**, 10956 (2016).
[11] J. Pan, C. Guo, C. Song, X. Lai, H. Li, W. Zhao, H. Zhang, G. Mu, K. Bu, T. Lin, X. Xie, M. Chen, and F. Huang, J. Am. Chem. Soc. **139**, 4623 (2017).
[12] Y. Ge and A. Y. Liu, Phys. Rev. B **82**, 155133 (2010).
[13] Y. Ge and A. Y. Liu, Phys. Rev. B **86**, 104101 (2012).
[14] P. Darancet, A. J. Millis, and C. A. Marianetti, Phys. Rev. B **90**, 045134 (2014).
[15] T. Ritschel, J. Trinckauf, K. Koepernik, B. Büchner, M. v. Zimmermann, H. Berger, Y. I. Joe, P. Abbamonte, and J. Geck, Nat. Phys. **11**, 328 (2015).
[16] P. Chen, Y.-H. Chan, M.-H. Wong, X.-Y. Fang, M. Y. Chou, S.-K. Mo, Z. Hussain, A.-V. Fedorov, and T.-C. Chiang, Nano Lett. **16**, 6331 (2016).
[17] E. Navarro-Moratalla, J. O. Island, S. Mañas-Valero, E. Pinilla-Cienfuegos, A. Castellanos-Gomez, J. Quereda, G. Rubio-Bollinger, L. Chirolli, J. A. Silva-Guillén, N. Agraït, G. A. Steele, F. Guinea, H. S. J. van der Zant, and E. Coronado, Nat. Commun. **7**, 11043 (2016).
[18] R. Hovden, A. W. Tsen, P. Liu, B. H. Savitzky, I. El Baggari, Y. Liu, W. Lu, Y. Sun, P. Kim, A. N. Pasupathy, and L. F. Kourkoutis, Proc. Natl. Acad. Sci. **113**, 11420 (2016).
[19] K. Dolui and S. Sanvito, Europhys. Lett. **115**, 47001 (2016).
[20] B. Sipos, A. F. Kusmartseva, A. Akrap, H. Berger, L. Forro, and E. Tutis, Nat. Mater **7**, 960 (2008).
[21] A. Spijkerman, J. L. de Boer, A. Meetsma, G. A. Wiegers, and S. van Smaalen, Phys. Rev. B **56**, 13757 (1997).
[22] K. Rossnagel, J. Phys.: Condens. Matter **23**, 213001 (2011).
[23] P. Fazekas and E. Tosatti, Philos. Mag. B **39**, 229 (1979).
[24] P. Fazekas and E. Tosatti, Physica B+C **99**, 183 (1980).
[25] B. Dardel, M. Grioni, D. Malterre, P. Weibel, Y. Baer, and F. Levy, Phys. Rev. B. **45**, 1462 (1992).
[26] B. Dardel, M. Grioni, D. Malterre, P. Weibel, Y. Baer, and F. Lévy, Phys. Rev. B **46**, 7407 (1992).
[27] L. Perfetti, P. A. Loukakos, M. Lisowski, U. Bovensiepen, M. Wolf, H. Berger, S. Biermann, and A. Georges, New J. Phys. **10**, 053019 (2008).
[28] S. Hellmann, M. Beye, C. Sohrt, T. Rohwer, F. Sorgenfrei, H. Redlin, M. Kalläne, M. Marczynski-Bühlow, F. Hennies, M. Bauer, A. Föhlisch, L. Kipp, W. Wurth, and K. Rossnagel, Phys. Rev. Lett. **105**, 187401 (2010).
[29] S. Hellmann, T. Rohwer, M. Kalläne, K. Hanff, C. Sohrt, A. Stange, A. Carr, M. Murnane, H. Kapteyn, L. Kipp, M. Bauer, and K. Rossnagel, Nat. Commun. **3**, 1069 (2012).
[30] K. T. Law and P. A. Lee, Proc. Natl. Acad. Sci. USA **114**, 6996 (2017).
[31] L. Balents, Nature (London) **464**, 199 (2010).
[32] M. Klanjšek, A. Zorko, R. Žitko, J. Mravlje, Z. Jagličić, P. K. Biswas, P. Prelovšek, D. Mihailovic, and D. Arčon, Nat. Phys. **13**, 1130 (2017).
[33] M. Kratochvilova, A. D. Hillier, A. R. Wildes, L. Wang, S.-W. Cheong, and J.-G. Park, npj Quantum Materials **2**, 42 (2017).
[34] A. Ribak, I. Silber, C. Baines, K. Chashka, Z. Salman, Y. Dagan, and A. Kanigel, Phys. Rev. B **96**, 195131 (2017).
[35] W.-Y. He, X. Y. Xu, G. Chen, K. Law, and P. A. Lee, Phys. Rev. Lett. **121**, 046401 (2018).
[36] M. B. Walker and R. L. Withers, Phys. Rev. B **28**, 2766 (1983).
[37] K. Nakanishi and H. Shiba, J. Phys. Soc. Jpn. **53**, 1103 (1984).
[38] S. Tanda, T. Sambongi, T. Tani, and S. Tanaka, J. Phys. Soc. Jpn. **53**, 476 (1984).
[39] M. Naito, H. Nishihara, and S. Tanaka, J. Phys. Soc. Jpn. **53**, 1610 (1984).
[40] M. Naito, H. Nishihara, and S. Tanaka, J. Phys. Soc. Jpn. **55**, 2410 (1986).
[41] T. Ishiguro and H. Sato, Phys. Rev. B **44**, 2046 (1991).
[42] G. A. Wiegers, J. L. de Boer, A. Meetsma, and S. van Smaalen, Z. für Kristallogr. - Cryst. Mater. **216**, 45 (2001).
[43] D. E. Moncton, F. J. DiSalvo, J. D. Axe, L. J. Sham, and B. R. Patton, Phys. Rev. B **14**, 3432 (1976).
[44] J. M. E. Portman, Ultrafast science: A multiscale modeling approach to femtosecond electron diffraction and its applications, Ph.D. thesis, Michigan State University, 2014.
[45] K. Koepernik and H. Eschrig, Phys. Rev. B **59**, 1743 (1999).
[46] R. Brouwer, Incommensurability in crystal structures, Ph.D. thesis, Rijksuniversiteit Groningen (Netherlands), 1978.
[47] J. P. Perdew, K. Burke, and M. Ernzerhof, Phys. Rev. Lett. **77**, 3865 (1996).
[48] J. P. Perdew and Y. Wang, Phys. Rev. B **45**, 13244 (1992).
[49] H. Eschrig, M. Richter, and I. Opahle, *Relativistic Solid State Calculations, in: Relativistic Electronic Structure Theory, Part 2. Applications*, edited by P. Schwerdtfeger (Elsevier, Amsterdam, 2004), Vol. 13, pp. 723–776.
[50] M. Bovet, S. van Smaalen, H. Berger, R. Gaal, L. Forró, L. Schlapbach, and P. Aebi, Phys. Rev. B **67**, 125105 (2003).
[51] J. A. Wilson, F. J. Di Salvo, and S. Mahajan, Phys. Rev. Lett. **32**, 882 (1974).
[52] Y. Liu, D. F. Shao, L. J. Li, W. J. Lu, X. D. Zhu, P. Tong, R. C. Xiao, L. S. Ling, C. Y. Xi, L. Pi, H. F. Tian, H. X. Yang, J. Q. Li, W. H. Song, X. B. Zhu, and Y. P. Sun, Phys. Rev. B **94**, 045131 (2016).
[53] D. Svetin, I. Vaskivskyi, S. Brazovskii, and D. Mihailovic, Sci. Rep. **7**, 46048 (2017).
[54] K. Rossnagel and N. V. Smith, Phys. Rev. B **73**, 073106 (2006).

[55] K. Rossnagel, E. Rotenberg, H. Koh, N. V. Smith, and L. Kipp, Phys. Rev. Lett. **95**, 126403 (2005).

[56] A. S. Ngankeu, S. K. Mahatha, K. Guilloy, M. Bianchi, C. E. Sanders, K. Hanff, K. Rossnagel, J. A. Miwa, C. B. Nielsen, M. Bremholm, and P. Hofmann, Phys. Rev. B **96**, 195147 (2017).

[57] F. Clerc, C. Battaglia, H. Cercellier, C. Monney, H. Berger, L. Despont, M. G. Garnier, and P. Aebi, J. Phys.: Condens. Matter **19**, 355002 (2007).

[58] A. Damascelli, Z. Hussain, and Z.-X. Shen, Rev. Mod. Phys. **75**, 473 (2003).

[59] W. Ku, T. Berlijn, and C.-C. Lee, Phys. Rev. Lett. **104**, 216401 (2010).

[60] A. Koitzsch, I. Opahle, S. Elgazzar, S. V. Borisenko, J. Geck, V. B. Zabolotnyy, D. Inosov, H. Shiozawa, M. Richter, M. Knupfer, J. Fink, B. Büchner, E. D. Bauer, J. L. Sarrao, and R. Follath, Phys. Rev. B **79**, 075104 (2009).

[61] M. Lindroos, S. Sahrakorpi, and A. Bansil, Phys. Rev. B **65**, 054514 (2002).

[62] M. Ligges, I. Avigo, D. Golež, H. U. R. Strand, Y. Beyazit, K. Hanff, F. Diekmann, L. Stojchevska, M. Kalläne, P. Zhou, K. Rossnagel, M. Eckstein, P. Werner, and U. Bovensiepen, Phys. Rev. Lett. **120**, 166401 (2018).

[63] T. Pillo, J. Hayoz, H. Berger, M. Grioni, L. Schlapbach, and P. Aebi, Phys. Rev. Lett. **83**, 3494 (1999).

[64] M. Bovet, D. Popovic, F. Clerc, C. Koitzsch, U. Probst, E. Bucher, H. Berger, D. Naumovic, and P. Aebi, Phys. Rev. B. **69**, 125117 (2004).

[65] S. V. Borisenko, A. A. Kordyuk, A. N. Yaresko, V. B. Zabolotnyy, D. S. Inosov, R. Schuster, B. Büchner, R. Weber, R. Follath, L. Patthey, and H. Berger, Phys. Rev. Lett. **100**, 196402 (2008).

[66] A. W. Tsen, R. Hovden, D. Wang, Y. D. Kim, J. Okamoto, K. A. Spoth, Y. Liu, W. Lu, Y. Sun, J. C. Hone, L. F. Kourkoutis, P. Kim, and A. N. Pasupathy, Proc. Natl. Acad. Sci. USA **112**, 15054 (2015).

[67] R. Hovden, P. Liu, N. Schnitzer, A. W. Tsen, Y. Liu, W. Lu, Y. Sun, and L. F. Kourkoutis, Microsc. Microanal. **24**, 387 (2018).